Measurement of dipolar cross-correlation in methylene groups in uniformly ^{13}C-, ^{15}N-labeled proteins

Yu Zheng & Daiwen Yang*
Department of Biological Sciences and Department of Chemistry, National University of Singapore, 14 Science Drive 4, Singapore 117543

Abstract

A CC(CO)NH TOCSY-based 3D pulse scheme is presented for measuring ^{1}H-^{13}C dipole-dipole cross-correlated relaxation at CH$_2$ positions in uniformly ^{13}C-, ^{15}N-labeled proteins. Simulations based on magnetization evolution under relaxation and scalar coupling interactions show that cross-correlation rates between ^{1}H-^{13}C dipoles in CH$_2$ groups can be simply obtained from the intensities of ^{13}C triplets. The normalized cross-correlation relaxation rates are related to cross-correlation order parameters for macromolecules undergoing isotropic motion, which reflect the degrees of spatial restriction of CH$_2$ groups. The study on human intestinal fatty acid binding protein (131 residues) in the presence of oleic acid demonstrates that side chain dynamics at most CH$_2$ positions can be characterized for proteins less than 15 kDa in size, with the proposed TOCSY-based approach.

Introduction

The availability of a large number of specific assignments for ^{15}N and ^{13}C resonances in proteins allows for the detailed study of dynamics of individual residues in a macromolecule through ^{2}H, ^{15}N or ^{13}C relaxation measurements (Muhandiram et al., 1995; Nesmelova et al., 2001; Palmer, 2001; Palmer et al., 1996). Such studies provide information on the location and energetics of the conformational changes in proteins and are important to the understanding of protein function (Eisenmesser et al., 2002; Wand, 2001). Data on dynamics can be obtained from auto- and/or cross-correlated relaxation experiments (Frueh, 2002; Kay, 1998).

Based on auto-correlated relaxation, side chain dynamics are characterized through the measurement of ^{13}C or ^{2}H relaxation times. However, due to ^{13}C-^{13}C scalar couplings and cross-correlated relaxation between ^{13}C-^{1}H dipoles in CH$_2$ and CH$_3$ groups, the application of ^{13}C relaxation to side chain dynamics is

greatly restricted. In this case, the measurement of ^{13}C relaxation in ^{12}C-^{13}CHD-^{12}C or ^{12}C-^{13}CHD$_2$ groups provides one with an opportunity to obtain dynamics of CH$_2$ and CH$_3$ groups in a protein sample with alternating ^{13}C-^{12}C labeling pattern, in concert with partial deuteration (LeMaster and Kushlan, 1996). Unlike ^{13}C and ^{1}H, ^{2}H relaxation is governed mainly by quadrupolar interaction and is insensitive to interactions with surrounding nuclei. A number of methods have been developed for measuring ^{2}H relaxation of methyl and methylene groups in uniformly ^{13}C-, fractionally ^{2}H-labeled samples (Millet et al., 2002; Muhandiram et al., 1995; Yang et al., 1998a). In contrast to the reasonable resolution of methyl groups in the ^{13}C-^{1}H correlation map to allow one to obtain the desired information, poor chemical shift dispersions of ^{13}C and ^{1}H in methylene and methine groups makes the use of ^{2}H relaxation problematic, particularly for medium and large proteins. Furthermore, in the measurement of ^{2}H relaxation in methylene and methine groups, dramatic signal loss can occur in magnetization transfer steps involving ^{2}H spin ($\sim$19 ms), due to the extremely short longitudinal relaxation times of the deuterons in these groups. As a result, measurements

*To whom correspondence should be addressed. E-mail: dbsydw@nus.edu.sg

of ^{2}H relaxation times are much more difficult in methylene and methine groups than in methyl groups. Finally, in terms of the efficiencies in cost and labor, approaches using both ^{2}H and ^{13}C are somewhat less advantageous, as additional sample preparation is required when the ^{13}C, ^{15}N samples used in structural characterization of proteins are not suitable.

Similar to auto-correlated relaxation, cross-correlated relaxation involving two distinct spin interactions depends on motional timescale and amplitude. This phenomenon was introduced as a means to obtain information on molecular dynamics around three decades ago (Mayne et al., 1976; Werbelow and Grant, 1975). However, it was only recently that cross-correlated relaxation effects in biomolecules became widely employed for a variety of purposes such as the improvement of spectral resolution and sensitivity (Pervushin et al., 1997), determination of molecular structure (Reif et al., 1997; Yang et al., 1997), and probing of molecular dynamics (Brutscher et al., 1997; Daragan et al., 1993; Engelke and Rüterjans, 1998; Ernst and Ernst, 1994; Fischer et al., 1997; Tjandra et al., 1996; Yang et al., 1998). Based on cross-correlated relaxation, a number of approaches have been proposed for the study of dynamics of heteronuclear multiple-spin systems (e.g., CH_2 and CH_3). One of them involves the measurement of initial decays of ^{13}C multiplet components from ^{13}C-^{1}H scalar coupled multiplets (Daragan et al., 1993; Mayne et al., 1976). In principle, auto- and cross-correlation spectral density functions can be obtained from relaxation times of ^{13}C multiplet components which can then be used to establish motional models and estimate motional time scales and amplitudes. This method, however, is applicable only to small molecules or specifically labeled macromolecules. Another approach is based on the detection of signal resulting from magnetization transfer mediated by cross-correlated relaxation (Engelke and Rüterjans, 1998; Ernst and Ernst, 1994). Although the sign of the signal can be used to discriminate between different motional regimes (Engelke and Rüterjans, 1998), quantitative information in this case is not easily accessible because auto-relaxation effects cannot be accounted for in a simple manner. Finally, yet another approach derives cross-correlated relaxation rates from the relative intensities of ^{13}C multiplet components. This approach, which can be viewed as the extension of the first method mentioned, was recently applied to methylene groups (Yang et al., 1998a). In the work, the problem of signal overlap was solved through the use of a 3D CBCA(CO)NH

scheme (incidentally, the use of this scheme limits the applicability of the method to C_β sites). Recently, we have developed a technique to measure methyl cross-correlated relaxation from ^{13}C multiplet intensities using a CC(CO)NH TOCSY (total correlation spectroscopy) scheme for magnetization transfer (Liu et al., 2003); the method has been successfully applied to the study of an intestinal fatty acid binding protein (IFABP) in the absence of fatty acid.

In the present paper, we propose an approach that affords characterization of methylene dynamics at all positions in the IFABP protein, through the measurement of dipolar cross-correlation using the CC(CO)NH TOCSY scheme. This new approach overcomes the problem of signal overlap and at the same time, does not require additional sample preparation as mentioned above. In our treatment, we examine in detail the effects of proton spin-flips and cross-correlated relaxation involving proton-proton and proton-carbon dipoles and chemical shift anisotropy (CSA) on the accuracy of the proposed method.
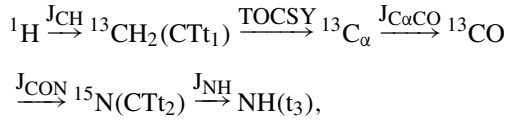
Materials and methods

NMR experiments were performed on a sample of 1.0 mM human intestinal fatty acid binding protein, pH 7.0, 90% H_2O, 10% D_2O, 25 °C and in the presence of 1.2 mM oleic acid. All experiments were recorded on a Bruker Avance DRX 500 MHz spectrometer equipped with an actively shielded cryoprobe and pulse field gradient units. To measure cross-correlated relaxation, 3D experiments were performed using the pulse scheme as shown in Figure 1. 16 scans were accumulated for each point in the indirect dimensions using a relaxation delay of one second. The 3D data were comprised of $151 \times 19 \times 512$ complex points with spectral widths of 6200, 1340 and 8000 Hz in ^{13}C, ^{15}N and ^{1}H dimensions, resulting in a total experimental time of 56 h. The data were apodized in the direct proton dimension with a sine weighting function shifted by 63°. The ^{15}N and ^{13}C time domains were doubled by mirror-image linear prediction prior to the application of a cosine-squared window function. After zero filling and Fourier transformation, the final data sets comprised of 1024, 128 and 768 points along the F3, F2 and F1 dimensions, respectively. Processing of the spectra was carried out using NMRPipe software (Delaglio et al., 1995). The spectra were analyzed using Pipp-capp software (Garrett et al., 1991).

Results and discussion

Pulse sequence

Figure 1 shows the pulse scheme for measuring cross-correlated relaxation between ^{13}C-^1H dipoles in CH_2 groups, using a uniformly ^{13}C-,^{15}N-labeled protein sample. The pulse sequence is similar to the CC(CO)NH TOCSY scheme (Montelione et al., 1992). The magnetization transfer is schematically shown as follows:

$$^1H \xrightarrow{J_{CH}} {}^{13}CH_2(CTt_1) \xrightarrow{TOCSY} {}^{13}C_\alpha \xrightarrow{J_{C\alpha CO}} {}^{13}CO$$

$$\xrightarrow{J_{CON}} {}^{15}N(CTt_2) \xrightarrow{J_{NH}} NH(t_3),$$

where CT t_i is a constant-time acquisition period.

In-phase ^{13}C magnetization (C_y) is generated at point a in the sequence through magnetization transfer from ^1H to ^{13}C followed by a period for anti-phase ^{13}C magnetization refocusing. Gradient g4 and the ^1H 90° pulse just before this gradient are applied to retain longitudinal magnetization C_z and destroy all other modes, except for zero-quantum coherence $C_z(H_{1+}H_{2-} + H_{1-}H_{2+})$. This is necessary to obtain a ^{13}C triplet with an intensity ratio of 1:2:1 for CH_2 groups in the absence of cross-correlated relaxation during the subsequent CT t_1 period. From point a to b, the ^{13}C magnetization is encoded with ^{13}C chemical shift, $^1J_{CH}$ coupling constant, and relaxation rates of the triplet components in CH_2 group. At the end of the constant-time period, a 90° pulse followed by gradient g5 suppresses all magnetization modes except C_z and $C_z(H_{1+}H_{2-} + H_{1-}H_{2+})$. Once again, this asserts a 1:2:1 pattern in the absence of cross-correlated relaxation. ^{13}C magnetization (C_z) is subsequently transferred to $C_{\alpha z}$ through cross-polarization during the TOCSY period from point c to point d in the sequence. On the other hand, magnetization $C_z(H_{1+}H_{2-} + H_{1-}H_{2+})$ cannot be transferred to $C_{\alpha z}$. Ultimately, the magnetization is transferred to amide ^{15}N and then to amide ^1H of the succeeding residue for detection.

Validation of the method

Due to cross-correlated relaxation, the triplet observed in F1 dimension deviates from a 1:2:1 pattern as expected for the ^{13}C spectrum of a CH_2 group under proton-carbon scalar coupling interaction. Assuming that each of the triplet components decays mono-exponentially, the dipole-dipole cross-correlation relaxation rate, $\Gamma_{CH1,CH2}$, can be approximated by the following expression (Yang et al., 1998a):

$$\Gamma_{CH1,CH2} \approx -[1/4T] \ln[4I_{out1} * I_{out2}/I_c^2], \quad (1)$$

where I_{out1}, I_{out2} and I_c are the intensities of the outer lines 1, 2 and the central line at the end of the constant-time period T. Note that the central line consists of two near-degenerate transitions. To validate the above approximation, relaxation of the multiplet components during the constant-time period T needs to be analyzed.

The three spins in a CH_2 group form an AX_2 or AMX system, depending on the equivalence of the two protons. Although there are four transitions for spin A in the AX_2 or AMX system, a triplet instead of a quartet is observed for CH_2 groups in the macromolecular limit due to the fact that difference of the two J_{CH} coupling constants (< 4 Hz) is small, compared to the line-width as will be discussed later. Per Equation 1, we are interested in the summation of the two inner transitions instead of individual transitions. Therefore, we can recast the two inner transitions, $\rho_{3,4}$ and $\rho_{5,6}$, into $(\rho_{3,4} + \rho_{5,6})/\sqrt{2}$ and $(\rho_{3,4} - \rho_{5,6})/\sqrt{2}$ as shown in the appendix where $(\rho_{3,4} + \rho_{5,6})/\sqrt{2}$ corresponds to the central line of the triplet. A similar treatment has also been employed for the AX_2 spin system by Prestegard and Grant (Prestegard and Grant, 1978). The evolution of the transverse magnetization of spin A during the constant-time period T can be described by:

$$\frac{dM}{dt} =$$

$$- \begin{bmatrix} i\omega_A + i\pi(J_{AM} + J_{AX}) + R_{11} & R_{12} \\ R_{21} & i\omega_A + R_{22} \\ R_{31} & i\pi(J_{AM} - J_{AX}) + R_{32} \\ R_{41} & R_{42} \end{bmatrix} \cdots$$

$$\cdots \begin{bmatrix} R_{13} & R_{14} \\ i\pi(J_{AM} - J_{AX}) + R_{23} & R_{24} \\ i\omega_A + R_{33} & R_{34} \\ R_{43} & i\omega_A - i\pi(J_{AM} + J_{AX}) + R_{44} \end{bmatrix}$$

$$\bullet \begin{bmatrix} M_1 \\ M_2 \\ M_3 \\ M_4 \end{bmatrix}, \quad (2)$$

where M is a vector consisting of magnetization M_i (i = 1, 2, 3 and 4); M_1 and M_4 represent the two outer lines while M_2 represents the central line $((\rho_{3,4} + \rho_{5,6})/\sqrt{2})$; M_3 corresponds to the difference between the two transitions within the central line
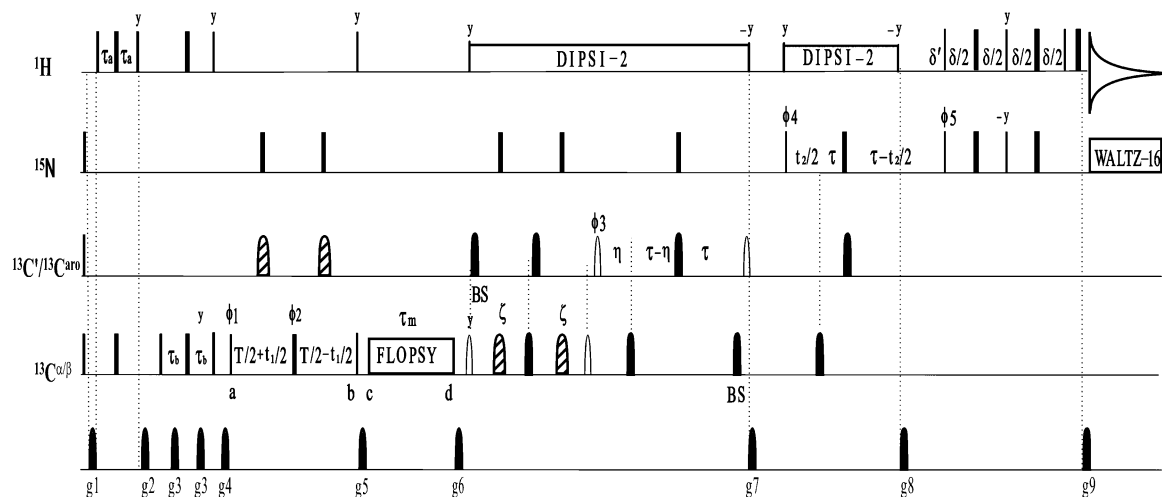
Figure 1. Pulse scheme for measuring cross-correlated relaxation rates in side chain methylene groups. All narrow (wide) rectangular pulses are applied with a flip angle of 90° (180°). The carriers are centered at 4.7 and 119 ppm for ^{1}H and ^{15}N, respectively. The ^{13}C carrier is set at 43 ppm until immediately prior to the ^{13}C'/^{13}C^{aro} pulse of phase ϕ_3 at which time the carrier is jumped to 176 ppm. All ^{1}H pulses are applied using a 40 kHz field while the ^{13}C rectangular pulses are applied with a 19.2 kHz field. All the ^{13}C shaped 90° pulses (opened shape) have the G4 profile (400 us, 11.7 kHz peak rf). All the ^{13}C shaped 180° pulses (filled shape) have the Q3 profile (Emsley and Bodenhausen, 1992) (300 μs, 11.0 kHz peak rf), except for the third shaped pulse on ^{13}C$^{\alpha/\beta}$ and sixth shaped pulse on ^{13}C'/^{13}C^{aro}. These two 180° shaped pulses have a REBURP profile with a maximum field of 15.6 kHz and duration of 400 μs. The ^{13}C$^{\alpha/\beta}$ shaped 180° pulses (shaded, 1.5 ms) applied in the middle of the delays ζ have the IBURP2 profile centered at 33 ppm with a bandwidth of 11.5 ppm. These decouple the ^{13}C$_\alpha-^{13}$C$_\beta$ couplings for most of residues. The ^{13}C'/^{13}C^{aro} shaped 180° pulses in the middle of the delays $T + t_1/2$ and $T - t_1/2$ refocus the ^{13}C-^{13}C' and ^{13}C-^{13}C$^\gamma$ (aromatic) couplings and are phase-modulated by 107 ppm. Bloch-Siegert compensation pulses are applied at the positions indicated by 'BS'. The ^{13}C spin-lock field strength for FLOPSY is 7 kHz. A ^{15}N decoupling power of 1 kHz was used during acquisition. Delays used were $\tau_a = 1.9$ ms; $\tau_b = 0.95$ ms; $T = 26$ ms; $\tau_m = 16$ ms; $\zeta = 3.8$ ms; $\eta = 4.5$ ms; $\tau = 12.4$ ms; δ' = 5.4 ms; $\delta = 4.6$ ms. The phase cycling used was: $\phi_1 = x$, $\phi_2 = x, y, -x, -y$; $\phi_3 = 2(x), 2(-x)$; $\phi_4 = 4(x), 4(-x)$; $\phi_5 = x$, rec $= x, -x, -x, x, -x, x, x, -x$. Quadrature detection in F1 dimension was achieved by State-TPPI of ϕ_1, while quadrature detection in F2 dimension used the enhanced sensitivity pulse field gradient method (Kay et al., 1992)where for each of t_2, separate data sets were recorded for (g8, ϕ_5) and ($-$g8, $\phi_5 + 180°$). For each successive t_2 value, ϕ_4 and the phase of the receiver were incremented by 180°. The duration and peak strengths of the sine-shaped gradients were: g1 = (1.5 ms, 20 G/cm); g2 = (2 ms, 25 G/cm); g3 = (0.5 ms, 20 G/cm); g4 = (1.5 ms, 35 G/cm); g5 = (2 ms, 30 G/cm); g6 = (1.5 ms, 25 G/cm); g7 = (1 ms, 30 G/cm); g8 = (1 ms, 40 G/cm); g9 = (1 ms, 4 G/cm).

$((\rho_{3,4} - \rho_{5,6})/\sqrt{2})$; R is a relaxation matrix; J_{AM} and J_{AX} are scalar coupling constants for bonds A-X and A-M in an AMX spin system. For an AX$_2$ spin system, $J_{AX} = J_{MX}$.

By considering three dipolar interactions (A-X, A-M, and M-X) and only the cross-correlation between A-X and A-M dipoles, the elements of matrix R for isolated AMX (and AX$_2$) systems have previously been derived (Kay and Bull, 1992; Prestegard and Grant, 1978). In addition to these contributions we took into account the remaining pairs of dipole-dipole cross-correlations (A-X/M-X and A-M/M-X) as well as dipole-CSA cross-correlations (A-X/A and A-M/A). The resulting complete expressions for the elements of matrix R are given in the appendix. In addition, dipolar interactions between protons in a CH$_2$ group and its proximal protons have been considered, although only auto-correlation terms were taken into account. It should be noted that the complete treatment based on Equation 2 proved to be of practical importance, as it can affect the interpretation of $\Gamma_{CH1,CH2}$ measurements (see below). The elements of the relaxation matrix R, together with eigenstates and transition frequencies, are listed in the appendix for AMX and AX$_2$ systems.

Due to cross-correlated and auto-correlated cross-relaxation, all magnetization modes in Equation 2 are coupled with each other. Each coherence M_i, generally speaking, decays in a multi-exponential manner. If the precession frequencies of coherences M_i and M_j differ by an amount that greatly exceeds the cross-relaxation term between these two modes (i.e., $|\omega_{ii} - \omega_{jj}| \gg R_{ij}$), then R_{ij} can be neglected in first-order approximation. This is similar to Redfield's secular approximation (Redfield, 1957). Keeping this approximation in mind, we can see that the two outer lines (M_1, M_4) relax in a mono-exponential manner. On the other hand, the precession frequencies of M_2 and M_3 may coincide

when $J_{AX} = J_{AM}$. In this case, the cross-relaxation term R_{23} which couples M_2 and M_3 gives rise to a bi-exponential decay for M_2. However, in practice the cross-term R_{23} is usually much smaller than the difference of the auto-relaxation rates, $R_{33} - R_{22}$, and can be safely ignored on these grounds (see explanation below).

Indeed, for an AX_2 system, the cross-relaxation rate R_{23} contains only spectral densities at high frequencies (ω_X, $\omega_X \pm \omega_A$), which are much smaller than that at zero-frequency in the macromolecular limit. At the same time, $R_{33} - R_{22} = 4/3 [J_{AX,AX}(0) - J_{AX}(0)] + R_{ZQ} - R_{1Xsel}$, where $J_{AX,AX}(0)$ and $J_{AX}(0)$ are cross- and auto-correlated spectral densities at zero-frequency (given in appendix), R_{ZQ} is the relaxation rate of zero-quantum coherence $X_{1+}X_{2-} + X_{1-}X_{2+}$ and R_{1Xsel} is the selective relaxation rate of longitudinal magnetization X_z measured under selective inversion of spin X. R_{ZQ} is dominated by spectral density $J(0)$ and can be considered to be the sum of transverse relaxation rates of spins X_1 and X_2, which is about 5 times as large as the proton spin-flip rate ($R_{ZQ} \approx 5 R_{1Xsel}$). Hence $R_{33} - R_{22}$ is dominated by the transverse relaxation rates of methylene protons and is normally much larger than R_{23} for protein systems. Therefore, the initial decay of the central line (M_2) during the constant-time period T is a single exponential in good approximation.

Similar conclusions can be drawn for an AMX system. The cross-relaxation term R_{23} in this case is equal to the difference of the two dipole/CSA rates, $\Gamma_{AM,A} - \Gamma_{AX,A}$. This quantity does not necessarily equal zero because the orientation of the two dipoles with respect to the CSA tensor may not be exactly identical. Since $\Gamma_{AM,A} - \Gamma_{AX,A}$ contains zero-frequency spectral density terms, R_{23}, hypothetically speaking, may become comparable to $R_{33} - R_{22}$. However, to our advantage, the amplitude of the mode M_3 (the difference of the two transitions within the central line) at point *a* in Figure 1 is zero. This largely eliminates any cross-relaxation transfer via R_{23}, leading to mono-exponential decay of M_2 over a relatively short time period T. This behavior is reminiscent of the initial magnetization decay in the case where a single mode is selectively excited while other modes are not disturbed. As shown below by means of numeric simulations, the mono-exponential decay remains an excellent approximation for T < 26 ms. Therefore, the intensities of triplet components in CH_2 spectra at time

T can be approximated as:

$$I_{out1} = \exp(-[\Gamma_{AX} + \Gamma_{AM} + \Gamma_{AM,AX} + \Gamma_{AM,A} + \Gamma_{AX,A} + \Gamma_A + 0.5J_{MX}(\omega_M) + 0.5J_{MX}(\omega_X) + 2J_{MX}(\omega_M + \omega_X) + 0.5(R_{1Msel} + R_{1Xsel})]T), \quad (3.1)$$

$$I_{out2} = \exp(-[\Gamma_{AX} + \Gamma_{AM} + \Gamma_{AM,AX} - \Gamma_{AM,A} - \Gamma_{AX,A} + \Gamma_A + 0.5J_{MX}(\omega_M) + 0.5J_{MX}(\omega_X) + 2J_{MX}(\omega_M + \omega_X) + 0.5(R_{1Msel} + R_{1Xsel})]T), \quad (3.2)$$

$$I_c = 2\exp(-[\Gamma_{AX} + \Gamma_{AM} - \Gamma_{AM,AX} + \Gamma_A + 0.5J_{MX}(\omega_M) + 0.5J_{MX}(\omega_X) + 0.5(R_{1Msel} + R_{1Xsel})]T), \quad (3.3)$$

where Γ_{AX} (Γ_{AM}) is the auto-relaxation rate attributed to dipole A-X (A-M); $\Gamma_{AM,AX}$ the cross-correlated relaxation rate between dipoles A-X and A-M; Γ_A the auto-relaxation rate attributed to CSA of spin A; $\Gamma_{AX,A}$ ($\Gamma_{AM,A}$) the cross-correlated relaxation rate between dipole AX (AM) and CSA of spin A; $J_{MX}(\omega)$ is the spectral density at frequency ω attributed to dipole M-X and R_{1Xsel} (R_{1Msel}) is the selective longitudinal relaxation rate of spin X (M). The expressions for relaxation rates and the definitions of spectral densities are given in the appendix. Based on Equation 3, we can calculate cross-correlation rates $\Gamma_{AX,AM}$ and $\Gamma_{AX,A} + \Gamma_{AM,A}$ as follows:

$$\Gamma_{AM,AX} = -[1/4T] \ln[4I_{out1}{}^*I_{out2}/I_c^2] - J_{MX}(\omega_M + \omega_X) \quad (4.1)$$
$$= 4/3J_{AM,AX}(0) + J_{AM,AX}(\omega_A), \quad (4.2)$$

$$\Gamma_{AM,A} + \Gamma_{AX,A} = -[1/2T] \ln[I_{out1}/I_{out2}] \quad (5.1)$$
$$= 4/3J_{AM,A}(0) + J_{AM,A}(\omega_A) + 4/3J_{AX,A}(0) + J_{AX,A}(\omega_A), \quad (5.2)$$

where $J_{ij,kl}(\omega)$ and $J_{ij,k}(\omega)$ are spectral densities as given in Appendix A. In the case where M = X, Equations 3–5 apply also to an AX_2 spin system. $J_{MX}(\omega_M + \omega_X)$ reaches a maximum value when $(\omega_M + \omega_X)\tau = 1$ and $\tau_m > 1$ ns, where $\tau = \tau_m\tau_e/(\tau_m + \tau_e)$; τ_m and τ_e are overall and internal correlation times, respectively. At 500 MHz proton frequency, the maximum value of $J_{MX}(\omega_M + \omega_X)$ is about 0.45 s^{-1} for highly

mobile CH_2 groups (M, X = H and order parameter of zero). $J_{MX}(\omega_M + \omega_X)$ decreases with increase of motional restriction in methylene groups. Therefore, $J_{MX}(\omega_M + \omega_X)$ can be neglected and the dipolar cross-correlated relaxation rate in a CH_2 group can be determined using Equation 1.

Second-order effect

In the first-order approximation, the effect of R_{ij} on the relaxation of M_i and M_j is negligible when $|\omega_{ii} - \omega_{jj}| \gg R_{ij}$ and $|\omega_{ii} - \omega_{jj}| \gg |R_{ii} - R_{jj}|$. In the second-order approximation, the decay of magnetization M_i can be described by (Ghose and Prestegard, 1998):

$$M_i(t) = e^{-R_{ii}t} \left\{ 1 - \frac{R_{ij}}{\omega_{ii} - \omega_{jj}} \sin\left[(\omega_{ii} - \omega_{jj})t\right] \right. $$
$$\left. e^{(R_{ii}-R_{jj})t} \right\}. \qquad (6)$$

When $\exp[(R_{ii} - R_{jj})t] \leq 1$ or $t = \pi n/(\omega_{ii} - \omega_{jj})$ where n is an integer number, the first-order approximation holds well. Assuming that $R_{ii} > R_{jj}$, the behavior of the coherence with a faster decay rate, $M_i(t)$, may deviate significantly from a single exponential when $(R_{ii} - R_{jj})t > 1.1$. However the component with a slower decay rate, $M_j(t)$, can still be described with good accuracy by a single exponential. This can be established by rewriting Equation 6 for $M_j(t)$ and observing that the second term in this expression is small. It is worth noting that with increase in protein size, the cross-relaxation terms R_{21} and R_{24} increase accordingly, such that the relaxation coupling between the inner and the outer lines of the triplet may, in principle, become appreciable.

Numerical simulations

To estimate the errors resulting from the two approximations described above (i.e., assumption of mono-exponential decay for all multiplet components and neglect of $J_{MX}(\omega_M + \omega_X)$), we assumed that the overall tumbling of the protein is isotropic and internal motion of the CH_2 group can be described by a model of restricted rotation about a single axis. This model applies to the rotational motion of a $C_\beta H_2$ group about the $C_\alpha C_\beta$ bond. For a simple model such as this, spectral density function $j_{ij,kl}(\omega)$ can be described by two parameters pertaining to internal motion – diffusion angular limit and diffusion constant, and a single parameter pertaining to overall motion (London and Avitabile, 1978). Alternatively, under the condition

that $\tau_m \gg \tau_e$, the density function $j_{ij,kl}(\omega)$ can be expressed as (Lipari and Szabo, 1982):

$$j_{ij,kl}(\omega) = S^2_{ij,kl}\tau_m / \left[1 + (\omega\tau_m)^2 \right]$$
$$+ \left[P_2(\cos\theta_{ij,kl}) - S^2_{ij,kl} \right]$$
$$\tau / \left[1 + (\omega\tau)^2 \right], \qquad (7)$$

where τ_m is the overall rotational time; τ_e is the correlation time of internal motion; $1/\tau = 1/\tau_m + 1/\tau_e$; $S^2_{a,b}$ is (cross- or auto-correlation) order parameter, which describes the degree of spatial restriction of vectors ij and kl; $P_2(\cos\theta_{ij,kl}) = 0.5(3\cos^2\theta_{ij,kl} - 1)$ where $\theta_{ij,kl}$ is the angle between vectors ij and kl. For auto-correlation (i.e., ij = kl), spectral density function and order parameter are denoted $j_{ij}(\omega)$ and S^2_{ij}, respectively. For CH_2 groups, auto- and cross-correlation order parameters are related to diffusion angular limit (γ) and are given by (Daragan and Mayo, 1995):

$$S^2_{CH} = 1/9 + (8/27)[(\sin\gamma/\gamma)^2(1 + $$
$$+ 2\cos^2\gamma)], \qquad (8.1)$$
$$S^2_{CH1,CH2} = 1/9 - (4/27)[(\sin\gamma/\gamma)^2(1 + $$
$$+ 2\cos^2\gamma)], \qquad (8.2)$$
$$S^2_{H1H2} = 1/4 + (3/4)[(\sin(2\gamma)/(2\gamma))^2], \quad (8.3)$$
$$S^2_{CH,H1H2} = 1/6 + (1/3)[(\sin(2\gamma)/(2\gamma))^2]. \quad (8.4)$$

A γ-value of 0° corresponds to no internal rotation, while a value of 180° corresponds to complete rotational freedom. The auto-correlation order parameters fall in the range from 0 to +1. The cross-correlation order parameter $S^2_{CH1,CH2}$ varies from $-1/3$ to $1/9$, while $S^2_{CH,H1H2}$ varies from $1/6$ to $1/2$. If the overall tumbling is anisotropic, Equations 7 and 8 are no longer valid. For CH_2 groups with multiple internal rotations, the expressions for the order parameters are much more complicated and involve multiple variables. However, the order parameters still fall within the same ranges as those for a single-rotational model, with the exception that $S^2_{CH,H1H2}$ spans the range from 0 to $1/2$ (Daragan and Mayo, 1997).

In our numerical simulations, the approximate cross-correlation rates were evaluated based on Equation 1 where the intensities of the triplet components were calculated numerically from Equation 2. The 'true' cross-correlation rates were obtained on the basis of corresponding spectral densities (Equation 4.2). The spectral density function throughout

the simulations was calculated from Equations 7 and 8. Proton spin-flip rates generally depend on proton density within the protein and the overall tumbling correlation time. For amide protons, for example, proton spin-flip rate is approximately $1*10^9\tau_m$ s^{-1}. For CH_2 protons, we assumed that $0.5*10^9\tau_m$ s^{-1} $\leq$ $R_{1Xsel} \leq 2*10^9\tau_m$ s^{-1} and $R_{ZQ} = 5\,R_{1Xsel}$. The initial conditions for equation 2 are considered separately for both AX_2 and AMX systems (see below).

For an AX_2 spin system exposed to the effects of the pulse sequence as shown in Figure 1, the initial intensity ratio of the triplet components, M_1:M_2:M_3:M_4, at point a in the sequence is 1:2:1:1. Note that the initial intensity of M_3, the difference of the two transitions within the central line, is not equal to zero in this case. For an AX_2 system then, M_3 actually corresponds to a multiple-quantum coherence (in operator notation, $A_y(X_{1+}X_{2-} + X_{1-}X_{2+})$). As shown in the section of pulse sequence, $C_z(H_{1+}H_{2-} + H_{1-}H_{2+})$ cannot be eliminated by application of rf pulses or field gradients in the situation where C_z needs to be retained, and thus results in the multiple-coherence at point a in the sequence. Although M_3 is not transferred for detection during the pulse sequence, it has the same precession frequency as M_2 and, therefore may affect the measurements of cross-correlations. The simulations carried out indicated that the difference between the approximate and 'true' rates was less than 0.4 s^{-1} in the cases when T = 26 ms, $0° \leq \gamma \leq 180°$, $1 \leq \tau_m \leq 12$ ns, $0 \leq \tau_e \leq 0.5$ ns and $J_{CH} = 135$ Hz, which is the average coupling constant in CH_2 groups. The difference is practically insensitive to motional parameters. Although the motional model is much more complicated for CH_2 groups with multiple rotations, the two outer lines still relax mono-exponentially since the condition of $|\omega_{ii} - \omega_{jj}| \ll R_{ij}$ holds better for the outer lines of ^{13}C triplets in CH_2 groups that are more flexible. It has been also found out that the cross-relaxation transfer between M_2 and M_3 is negligible during a short relaxation period (T $\leq$ 26 ms). The major source of error here results from the omission of $J_{H1H2}(\omega_{H1} + \omega_{H2})$. Nonetheless, Equation 1 is a good approximation for obtaining the dipolar cross-correlation rates in AX_2 systems. However, when cross-correlated order parameter $S^2_{CH1,CH2}$ approaches zero or when protein size is small ($\tau_m < 3$ ns), the unwanted contribution of $J_{H1H2}(\omega_{H1} + \omega_{H2})$ to the rate determined from Equation 1 is not insignificant.

Next, let us consider an AMX system where $J_{AX} = J_{AM}$. The initial intensity ratio of M_1:M_2:M_3:M_4 at point a in the sequence is 1:2:0:1. For an AMX system, M_3 corresponds to the difference of two single-quantum coherences (in operator notation, $A_y(M_z - X_z)$) instead of a multiple-coherence. In this case, R_{23} may be comparable to $R_{22} - R_{33}$, suggesting that the decay of M_2 may deviate significantly from a mono-exponential profile. To estimate the error resulting from mono-exponential approximation, we used a maximum attainable R_{23} value in our simulation. Using the principal components of CSA tensors from solid state NMR studies of amino acids (Ye et al., 1993), the maximum value was searched from among 20 amino acids by varying the orientation of C-H dipoles of a CH_2 group, with respect to the CSA tensor, by performing a rotation about the C-C bond. A maximum value of $R_{23} = \Gamma_{CH1,C} - \Gamma_{CH2,C}$ was found to be about 7 s^{-1} for a CH_2 group fixed in a rigid spherical molecule with an overall tumbling correlation time of 4 ns. Since R_{23} is dominated by spectral density at zero-frequency, it scales linearly with τ_m for proteins of larger sizes. Similar to the AX_2 system, deviation of the cross-correlation rate obtained with Equation 1 from the 'true' one can be calculated with T = 26 ms, $0° \leq \gamma \leq 180°$, $1 \leq \tau_m \leq 12$ ns, $0 \leq \tau_e \leq 0.5$ ns, $0.5*10^9\tau_m \leq R_{1Xsel} \leq 2*10^9\tau_m$ s^{-1}, $|\Gamma_{CH1,C} - \Gamma_{CH2,C}| = 7*(10^9\tau_m/4)$ s^{-1} and $J_{CH} = 135$ Hz. It has been found that the deviation is almost insensitive to R_{1Xsel} and τ_e and that it reaches a maximum when $\tau_e = 0.16$ ns. Figure 2 shows how the apparent value of cross-correlation differs from the 'true' one as a function of the overall rotational time (τ_m) and diffusion restriction (γ) for $\tau_e = 0.16$ ns and $R_{1Xsel} = 1.5*10^9\tau_m$ s^{-1}. The difference between the approximate and 'true' rates is less than 0.4 s^{-1} for $\tau_m < 9$ ns. The difference can be larger when the protein size is large ($\tau_m > 9$ ns), due to second-order effects as illustrated in Equation 6. However, the fractional error in $\Gamma_{CH1,CH2}$ is still very small ($< 3\%$).

In the case where $J_{AX} \neq J_{AM}$, four peaks should, in principle, be observed. To estimate the difference of the two $^1J_{CH}$ coupling constants in a CH_2 group where its two protons are magnetically distinguishable, we measured the $^1J_{CH}$ values from an HBHA(CBCACO)NH experiment without ^{13}C decoupling during the chemical shift evolution periods of HB and HA spins, using an IFABP sample. The difference between $^1J_{CH1}$ and $^1J_{CH2}$ in CH_2 groups was found to be less than 4 Hz. Due to cross-correlated relaxation between C-H dipole and a second dipolar interaction involving the methylene proton and one of its proximal spins, the J_{CH} constants measured in this
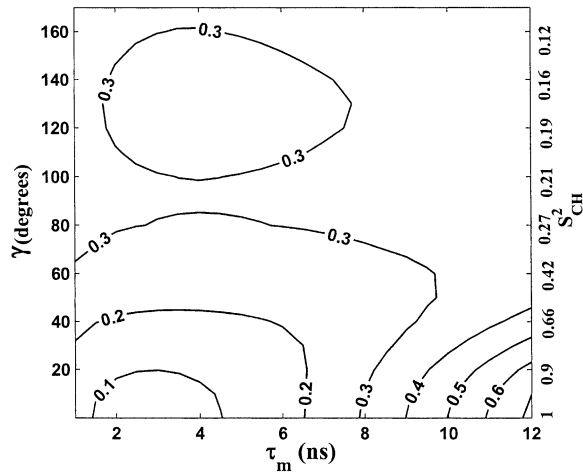
Figure 2. Comparison of $\Gamma_{CH1,CH2}$ and $\Gamma_{CH1,CH2}$(true). $\Gamma_{CH1,CH2}$ is derived from numerical simulations using Equations 1 and 2. $\Gamma_{CH1,CH2}$(true) is derived according to Equation 4.2. The difference, $\Gamma_{CH1,CH2} - \Gamma_{CH1,CH2}$(true), shown in the contour plot is calculated with $\tau_e = 0.16$ ns. τ_e values other than 0.16 ns lead to the difference that is smaller than the one indicated in the plot for the given ranges of τ_m (overall correlation time) and γ (diffusion angular limit) values.

manner are subject to small errors. However, the true difference between $^1J_{CH1}$ and $^1J_{CH2}$ should not significantly exceed 4 Hz (Yang et al., 1998b). Therefore, the two inner lines cannot be resolved given the small difference in their frequencies. Note that the slight difference in frequencies between the two components of the central line makes the cross-relaxation between these two components less effective. In this sense, Equation 1 is a better approximation for the case where $J_{AX} \neq J_{AM}$ than for the case where $J_{AX} = J_{AM}$. In our previous and present experiments, the ^{13}C resonances were recorded in a constant-time mode so that all signals in the ^{13}C dimension have the same line-width. As a result, peak heights can be equated with signal intensities. When the two components of the central line are slightly shifted with respect to each other, the observed peak height may differ from the sum of two individual heights. Numerical simulations indicate that the resulting error in peak height is less than 1.5% when the separation of the two components is less than 6 Hz. A 1.5% underestimation of the central peak intensity results in about 0.3 s^{-1} overestimation of $\Gamma_{CH1,CH2}$ for T = 26 ms. Therefore, Equation 1 can be considered a reliable approximation for obtaining dipole-dipole cross-correlated relaxation rates in CH_2 groups in proteins.

Table 1. Dipole-dipole cross-correlated relaxation rates of lysine residues in the human intestinal fatty acid binding protein in the presence of oleic acid

Residue	$\Gamma_{CH1,CH2}(s^{-1})$	$\delta\Gamma_{CH1,CH2}$ (s^{-1})*	S'	δS'
K7C$_\beta$	−0.91	0.85	0.04	0.04
K7C$_\gamma$	0.63	0.60	−0.03	0.03
K7C$_\delta$	1.28	0.97	−0.05	0.04
K7C$_\varepsilon$	2.38	1.67	−0.10	0.07
K16C$_\beta$	−2.37	0.72	0.10	0.03
K16C$_\gamma$	−0.01	0.38	0.0	0.02
K16C$_\delta$	1.67	0.83	−0.07	0.04
K16C$_\varepsilon$	−3.00	1.24	0.13	0.05
K20C$_\beta$	−19.07	3.02	0.82	0.13
K27C$_\beta$	−7.13	1.02	0.31	0.04
K27C$_\gamma$	2.05	0.61	−0.09	0.03
K27C$_\delta$	−3.31	1.38	0.14	0.06
K27C$_\varepsilon$	3.07	1.84	−0.13	0.08
K29C$_\beta$	−4.26	0.69	0.18	0.03
K29C$_\gamma$	0.43	0.44	−0.02	0.02
K29C$_\delta$	−0.83	0.83	0.04	0.04
K29C$_\varepsilon$	3.08	1.32	−0.13	0.06
K37C$_\beta$	1.71	0.90	−0.07	0.04
K37C$_\gamma$	1.30	0.73	−0.06	0.03
K37C$_\delta$	3.04	1.17	−0.13	0.05
K37C$_\varepsilon$	7.30	1.97	−0.31	0.08
K46C$_\beta$	−5.13	0.91	0.22	0.04
K46C$_\gamma$	−2.88	0.60	0.12	0.03
K46C$_\delta$	3.04	1.07	−0.13	0.05
K46C$_\varepsilon$	7.08	1.59	−0.30	0.07
K50C$_\gamma$	0.17	1.19	−0.01	0.05
K50C$_\delta$	−2.17	1.82	0.09	0.08
K50C$_\varepsilon$	3.47	2.37	−0.15	0.10
K88C$_\beta$	−9.33	1.72	0.40	0.07
K88C$_\varepsilon$	−0.18	2.28	0.01	0.10
K92C$_\beta$	−3.24	1.34	0.14	0.06
K92C$_\gamma$	0.48	0.65	−0.02	0.03
K92C$_\delta$	−0.08	0.95	0.0	0.04
K92C$_\varepsilon$	−4.23	1.68	0.18	0.07
K94C$_\beta$	−2.41	0.89	0.10	0.04
K94C$_\gamma$	2.73	0.56	−0.12	0.02
K94C$_\delta$	6.14	1.01	−0.26	0.04
K94C$_\varepsilon$	0.82	1.35	−0.04	0.06
K125C$_\beta$	2.26	1.84	−0.10	0.08
K125C$_\gamma$	5.72	1.51	−0.25	0.06
K129C$_\beta$	−10.99	1.29	0.47	0.06
K129C$_\gamma$	−5.37	0.93	0.23	0.04
K129C$_\delta$	−2.07	1.35	0.09	0.06
K129C$_\varepsilon$	0.60	1.95	−0.03	0.08
K130C$_\beta$	1.43	0.53	−0.06	0.02
K130C$_\gamma$	4.84	0.45	−0.21	0.02
K130C$_\delta$	2.85	0.94	−0.12	0.04
K130C$_\varepsilon$	2.08	1.38	−0.09	0.06

*$\delta\Gamma_{CH1,CH2}$ and δS' are errors for $\Gamma_{CH1,CH2}$ and S', respectively. They were estimated from the uncertainty of the triplet intensity (I_{out1}, I_{out2} and I_c).

Application to human intestinal fatty acid binding protein (IFABP)

Using the pulse sequence shown in Figure 1, we measured the dipole-dipole cross-correlation rates of CH_2 groups in human intestinal fatty acid binding protein in the presence of oleic acid. Figure 3 shows the F1 ^{13}C slices for residues Lys129 and Lys130. Four triplets were observed for four CH_2 groups in each lysine residue as expected. $^{13}C_\epsilon$ is scalar coupled to an odd number of carbons while carbon spins from all other sites are coupled to an even number. Hence, the sign of the $^{13}C_\epsilon$ signal is opposite to that of the other carbons. Due to cross-correlated relaxation, intensities of the triplet components deviate from the pattern of 1:2:1. Using peak intensities (heights), the dipole-dipole cross-correlation rates, $\Gamma_{CH1,CH2}$, were calculated according to Equation 1. Although lysine residues possess very long side chains, causing relatively inefficient TOCSY transfer, the S/N ratios are sufficient to provide information on dynamics for most lysines in IFABP (131 residues, overall rotational time of 8 ns). Table 1 lists the cross-correlated relaxation rate constants for lysine residues. In general, the CH_2 groups residing in side chains shorter than lysine show better sensitivity in the spectra recorded with the sequence of Figure 1. In total, we obtained $\Gamma_{CH1,CH2}$ values for 74 out of 111 CH_2 groups from non-lysine residues. Some multiplets showed phase distortions due to the effect of strong coupling between ^{13}C spins – these residues were not included in the analyses. Other multiplets registered very low intensities and were likewise omitted. It is noteworthy that reliable data were obtained for most of the aromatic residues although auto-correlated relaxation rates for these residues tend to be very large because of the highly restricted internal motion. We conclude that the proposed method can be successfully applied to proteins with overall rotational correlation times of 8 ns or less.

The dipole-dipole cross-correlated relaxation rate depends on both overall and internal motions. To probe internal dynamics from relaxation data, a motional model is required. While many models have been proposed over the last several years (Bremi and Bruschweiler, 1997; for reviews, see Daragan and Mayo, 1997; Frueh, 2002; Korzhnev et al., 2001), all of them require two or more parameters for parameterization of internal motion. In our situation where only one piece of experimental data is available for each CH_2 group, we define a normalized cross-correlation
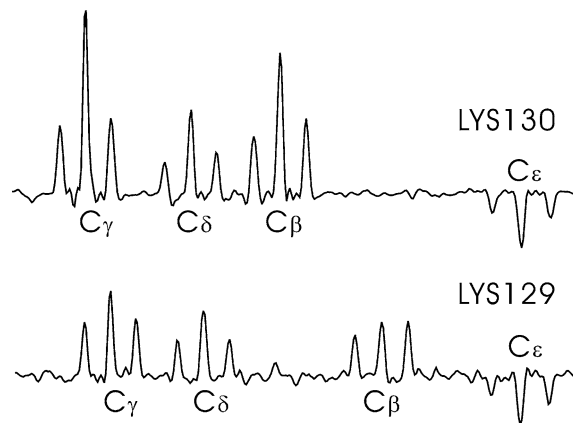

Figure 3. F1 ^{13}C cross-sections from data recorded on an ^{15}N-, ^{13}C-labeled human fatty acid binding protein in the presence of oleic acid. Each carbon in the side chain CH_2 group gives rise to a triplet resulting from one-bond scalar coupling interaction. Cross-correlated relaxation interactions make the triplet deviate from a pattern of 1:2:1 intensity ratio.

rate as:

$$S' = \Gamma^{exp}_{CH1,CH2} / \Gamma^{rigid}_{CH1,CH2}, \qquad (9)$$

where $\Gamma^{rigid}_{CH1,CH2}$ is the value of $\Gamma_{CH1,CH2}$ in the absence of internal motions and equals -23.3 s^{-1} for holo-IFABP at 25 °C; $\Gamma^{exp}_{CH1,CH2}$ is the cross-correlation rate measured experimentally according to Equation 1 and approximates the equation 4/3 $J_{CH1,CH2}(0) + J_{CH1,CH2}(\omega_C) + J_{H1H2}(\omega_{H1} + \omega_{H2})$. It has been shown that S' correlates with the order parameter obtained from deuterium relaxation times when the overall tumbling motion is nearly isotropic (Yang et al., 1998a). When contributions of internal motions and spectral densities $J_{CH1,CH2}(\omega_C)$ and $J_{H1H2}(\omega_{H1} + \omega_{H2})$ to $\Gamma^{exp}_{CH1,CH2}$ are negligible, S' is reduced to $S^2_{CH1,CH2}/P_2(\cos\beta)$, where β is the angle between the two H-C dipoles in CH_2 group (109.5°). Numerical simulations conducted indicate that S' correlates very well with $S^2_{CH1,CH2}/P_2(\cos\beta)$ in the case of isotropic overall motion. In these simulations, the values of $S^2_{CH1,CH2}$ used were in the range from $-1/3$ to $1/9$ and S' was calculated according to Equation 9. For side chains restricted in motions, S' is slightly smaller than $S^2_{CH1,CH2}/P_2(\cos\beta)$. On the other hand, for highly flexible side chains S' is somewhat larger than $S^2_{CH1,CH2}/P_2(\cos\beta)$. The comparison of S' and $S^2_{CH1,CH2}$ is shown in the contour plot in Figure 4 for $\tau_e = 0.25$ ns. The larger the τ_e value, the larger the difference between S' and $S^2_{CH1,CH2}/P_2(\cos\beta)$. It must be emphasized that the good correlation between S'
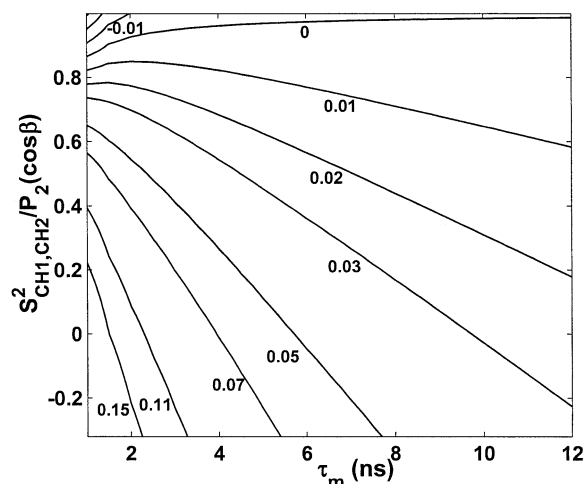
Figure 4. Comparison of S' and $S^2_{CH1,CH2}$. S' is obtained using Equation 9. The value of $S^2_{CH1,CH2}$ used was in the range of $-1/3$ to $1/9$, with intervals of 0.01. The difference, $S' - S^2_{CH1,CH2}/P_2(\cos\beta)$ where $P_2(\cos\beta) = 0.5(3\cos^2\beta - 1)$ and $\beta = 109.5°$, shown in the contour plot is calculated with $\tau_e = 0.25$ ns.

and $S^2_{CH1,CH2}$ is limited to proteins with isotropic or slightly anisotropic overall tumbling. For proteins with overall rotational correlation times larger than 4 ns and internal correlation times less than 0.25 ns, the difference between S' and $S^2_{CH1,CH2}/P_2(\cos\beta)$ is quite small (absolute value less than 0.09), especially in cases where $S^2_{CH1,CH2}/P_2(\cos\beta) > 0$. For smaller proteins, or for highly mobile side chains, $\Gamma_{CH1,CH2}$ alone cannot provide an accurate measure of the amplitude of internal motion. In this case, meaningful interpretation can be obtained in combination with relaxation time T_1 and heteronuclear NOE.

Table 1 shows the normalized cross-correlation rates, S', defined according to Equation 9. Except for K20, all of the lysine residues possess very flexible side chains. This is consistent with the structure determined by NMR where all lysine residues reside on the outer surface of the protein (Zhang et al., 1997). The S' value for $C_\beta H_2$ group in K20 is close to the maximum value of 1, indicating that the rotation about χ_1 torsion angle is highly restricted. Other CH_2 groups in K20 produce insufficient signals for the measurement of cross-correlation rates. This implies that the rotations of these CH_2 groups are also restricted, resulting in short relaxation times and concomitant signal loss during the TOCSY period. Solution NMR structures show the existence of side chain - side chain interactions between K20 and V122 (Zhang et al., 1997). The terminal of K20 may also interact with

E120 through charge-charge interaction since the two side chains are very close to each other. This suggestion is supported by the high rigidity of the side chain of E120 (S' (C_β) = 0.72 and S' (C_γ) = 0.54).

For a given lysine side chain with uninhibited rotations about the C-C bonds, the magnitude of S' declines dramatically along the side chain towards the terminus ($S^2 = 1/9^N$, where N is the number of dihedral angles intervening between the site of interest and C_α). According to the data in Table 1, none of the lysine residues display such an absolute motional freedom. In majority of cases, the mobility of the side chain increases towards the end of the side chain. A number of exceptions have been observed, however, such as K16 and K27, which can be attributed to side chain – backbone and/or side chain – side chain interactions.

Conclusion

In conclusion, dipole–dipole cross-correlated relaxation rate in a CH_2 group can be approximated using the intensities of the components in ^{13}C triplet according to $\Gamma_{CH1,CH2} = -[1/4T]\ln[4I_{out1}*I_{out2}/I_c^2]$. Numerical simulations conducted indicate that the rate determined from peak intensities is larger than the true rate, but the difference is less than 0.4 s^{-1} when $\tau_m < 9$ ns. Although the absolute error in $\Gamma_{CH1,CH2}$ can be larger than 0.4 s^{-1} when $\tau_m > 9$ ns and internal motions are restricted, the fractional error does not exceed 3%. The normalized cross-correlated relaxation rate obtained from Equation 9 correlates very well with the cross-correlation order parameter $S^2_{CH1,CH2}$, which reflects the degree of spatial restraint of the side chain. The experiment proposed here allows one to obtain information on local dynamics for a majority of CH_2 sites in the protein. Although the method is limited by sensitivity due to the application of TOCSY transfer; with the availability of cryoprobe technology, it can be applied to proteins with overall rotational correlation times of around 8 ns or less. In contrast to ^2H relaxation studies, the present approach requires only a ^{13}C-, ^{15}N-labeled sample that is used for structural studies. Moreover, spectra recorded with the proposed pulse sequence do not encounter problems caused by poor chemical shift dispersion of the ^1H and ^{13}C nuclei, characteristic of side chain CH_2 groups. In application to human intestinal fatty acid binding protein, side chain dynamics varies substantially (S' from -0.3 to $\sim$1), even among amino acids of the same type.

Information on side chain dynamics obtained in this manner is expected to provide valuable insights into protein folding, stability and function.

Appendix A

Eigenstates, carbon transitions and transverse relaxation matrix elements for AMX and AX_2 spin systems where $A = {}^{13}C$, M, $X = {}^{1}H$.

The first spin state in wave function $|k>$ corresponds to the ^{13}C spin state and the remaining spin states are associated with the proton spins.

1. AMX spin system

Eigenstates

$$|1 >= \beta\alpha\alpha \qquad |2 >= \alpha\alpha\alpha \qquad |3 >= \beta\alpha\beta \qquad |4 >= \alpha\alpha\beta$$

$$|5 >= \beta\beta\alpha \qquad |6 >= \alpha\beta\alpha \qquad |7 >= \beta\beta\beta \qquad |8 >= \alpha\beta\beta$$

Transitions ($\rho_{i,j} = |i><j|$) and frequencies for spin A

$$\rho_{1,2} \qquad \omega_1 = \omega_A - \pi J_{AM} - \pi J_{AX}$$
$$\rho_{3,4} \qquad \omega_2 = \omega_A - \pi J_{AM} + \pi J_{AX}$$
$$\rho_{5,6} \qquad \omega_3 = \omega_A + \pi J_{AM} - \pi J_{AX}$$
$$\rho_{7,8} \qquad \omega_4 = \omega_A + \pi J_{AM} + \pi J_{AX}$$

Basis for relaxation matrix R

$$M_1 = \rho_{1,2}$$
$$M_2 = (\rho_{3,4} + \rho_{5,6})/\sqrt{2}$$
$$M_3 = (\rho_{3,4} - \rho_{5,6})/\sqrt{2}$$
$$M_4 = \rho_{7,8}$$

Transverse relaxation matrix elements for spin A

$$R_{11} = \Gamma_{AX} + \Gamma_{AM} + \Gamma_{AM,AX} + \Gamma_{AM,A} + \Gamma_{AX,A} + \Gamma_A + 2J_{MX}(\omega_M + \omega_X) + 0.5J_{MX}(\omega_M) + 0.5J_{MX}(\omega_X)$$
$$+ 0.5(R_{1Msel} + R_{1Xsel})$$

$$R_{12} = \sqrt{2}/4[J_{AX}(\omega_X) + J_{AM}(\omega_M) - J_{MX}(\omega_X) - J_{MX}(\omega_M) - 2J_{AX,MX}(\omega_X) - 2J_{AM,MX}(\omega_M)$$
$$- (R_{1Msel} + R_{1Xsel})]$$

$$R_{13} = \sqrt{2}/4[J_{AX}(\omega_X) - J_{AM}(\omega_M) - J_{MX}(\omega_X) + J_{MX}(\omega_M) - 2J_{AX,MX}(\omega_X) + 2J_{AM,MX}(\omega_M)$$
$$+ (R_{1Msel} - R_{1Xsel})]$$

$$R_{14} = -2J_{MX}(\omega_M + \omega_X)$$

$$R_{22} = \Gamma_{AX} + \Gamma_{AM} - \Gamma_{AM,AX} + \Gamma_A + 0.5J_{MX}(\omega_M) + 0.5J_{MX}(\omega_X) + 0.5(R_{1Msel} + R_{1Xsel})$$

$$R_{23} = \Gamma_{AM,A} - \Gamma_{AX,A}$$

$$R_{24} = \sqrt{2}/4[J_{AX}(\omega_X) + J_{AM}(\omega_M) - J_{MX}(\omega_X) - J_{MX}(\omega_M) + 2J_{AX,MX}(\omega_X) + 2J_{AM,MX}(\omega_M)$$
$$- (R_{1Msel} + R_{1Xsel})]$$

$$R_{33} = \Gamma_{AX} + \Gamma_{AM} - \Gamma_{AM,AX} + \Gamma_A + 2/3J_{MX}(\omega_M - \omega_X) + 0.5J_{MX}(\omega_M) + 0.5J_{MX}(\omega_X)$$
$$+ 0.5(R_{1Msel} + R_{1Xsel})$$

$$R_{34} = \sqrt{2}/4[-J_{AX}(\omega_X) + J_{AM}(\omega_M) + J_{MX}(\omega_X) - J_{MX}(\omega_M) - 2J_{AX,MX}(\omega_X) + 2J_{AM,MX}(\omega_M)$$
$$- (R_{1Msel} - R_{1Xsel})]$$

$$R_{44} = \Gamma_{AX} + \Gamma_{AM} + \Gamma_{AM,AX} - \Gamma_{AM,A} - \Gamma_{AX,A} + \Gamma_A + 0.5J_{MX}(\omega_M) + 0.5J_{MX}(\omega_X) + 2J_{MX}(\omega_M + \omega_X)$$
$$+ 0.5(R_{1Msel} + R_{1Xsel})$$

$$R_{ij} = R_{ji}$$

2. AX$_2$ system
Eigenstates

$$|1> = \beta\alpha\alpha \qquad |2> = \alpha\alpha\alpha \qquad |3> = \beta(\alpha\beta + \beta\alpha)/\sqrt{2} \qquad |4> = \alpha(\beta\alpha + \alpha\beta)/\sqrt{2}$$

$$|5> = \beta(\alpha\beta - \beta\alpha)/\sqrt{2} \qquad |6> = \alpha(\alpha\beta - \beta\alpha)/\sqrt{2} \qquad |7> = \beta\beta\beta \qquad |8> = \alpha\beta\beta$$

Transitions and frequencies for spin A

$$M_1 = \rho_{1,2} \qquad\qquad \omega_1 = \omega_A - 2\pi J_{AX}$$
$$M_2 = (\rho_{3,4} + \rho_{5,6})/\sqrt{2} \qquad \omega_2 = \omega_A$$
$$M_3 = (\rho_{3,4} - \rho_{5,6})/\sqrt{2} \qquad \omega_3 = \omega_A$$
$$M_4 = \rho_{7,8} \qquad\qquad \omega_4 = \omega_A + 2\pi J_{AM}$$

Transverse relaxation matrix elements of spin A

$$R_{11} = 2\Gamma_{AX} + \Gamma_{AX,AX} + 2\Gamma_{AX,A} + \Gamma_A + J_{XX}(\omega_X) + 2J_{XX}(2\omega_X) + R_{1Xsel}$$

$$R_{12} = \sqrt{2}/4[2J_{AX}(\omega_X) - 2J_{XX}(\omega_X) - 4J_{AX,XX}(\omega_X) - 2R_{1Xsel}]$$

$$R_{13} = \sqrt{2}/4[2J_{AX,AX}(\omega_X) - 2J_{XX}(\omega_X) - 4J_{AX,XX}(\omega_X)]$$

$$R_{14} = -2J_{XX}(2\omega_X)$$

$$R_{22} = 2\Gamma_{AX} - \Gamma_{AX,AX} + \Gamma_A + J_{XX}(\omega_X) + R_{1Xsel}$$

$$R_{23} = J_{XX}(\omega_X) + 1/3J_{AX,AX}(\omega_A - \omega_X) + J_{AX,AX}(\omega_X) + 2J_{AX,AX}(\omega_A + \omega_X)$$

$$R_{24} = \sqrt{2}/4[2J_{AX}(\omega_X) - 2J_{XX}(\omega_X) + 4J_{AX,XX}(\omega_X) - 2R_{1Xsel}]$$

$$R_{33} = 2\Gamma_{AX} - \Gamma_{AX,AX} + \Gamma_A - 4/3[J_{AX}(0) - J_{AX,AX}(0)] + J_{XX}(\omega_X) + R_{ZQ}$$

$$R_{34} = \sqrt{2}/4[2J_{AX,AX}(\omega_X) - 2J_{XX}(\omega_X) + 4J_{AX,XX}(\omega_X)]$$

$$R_{44} = 2\Gamma_{AX} + \Gamma_{AX,AX} - 2\Gamma_{AX,A} + \Gamma_A + J_{XX}(\omega_X) + 2J_{XX}(2\omega_X) + R_{1Xsel}$$

$$R_{ij} = R_{ji}$$

3. Notations used in the relaxation elements

$$\Gamma_{AM} = 2/3J_{AM}(0) + 1/6J_{AM}(\omega_A - \omega_M) + 1/2J_{AM}(\omega_A) + 1/2J_{AM}(\omega_M) + J_{AM}(\omega_A + \omega_M)$$

$$\Gamma_{AM,AX} = 4/3J_{AM,AX}(0) + J_{AM,AX}(\omega_A)$$

$$\Gamma_{AM,A} = 4/3J_{AM,A}(0) + J_{AM,A}(\omega_A)$$

$$\Gamma_A = 4/3J_A(0) + J_A(\omega_A)$$

$$J_{ij,kl}(\omega) = 0.3(\mu_0\gamma_i\gamma_j h/(8\pi^2 r_{ij}^3))(\mu_0\gamma_k\gamma_l h/(8\pi^2 r_{kl}^3))j_{ij,kl}(\omega)$$

$$J_{ij}(\omega) = J_{ij,ij}(\omega)$$

$$J_{ij,i}(\omega) = 0.2[\mu_0\gamma_i\gamma_j h/(8\pi^2 r_{ij}^3)][\omega_i(P_2(\cos X)\sigma_X + P_2(\cos Y)\sigma_Y + P_2(\cos Z)\sigma_Z]j_{ij,i}(\omega)$$

$$J_A(\omega) = 1/15\omega_A^2(\sigma_X^2 + \sigma_Y^2 + \sigma_Z^2 - \sigma_X\sigma_Y - \sigma_X\sigma_Z - \sigma_Y\sigma_Z)j_{A,A}(\omega)$$

$$j_{ij,kl}(\omega) = S_{ij,kl}^2\tau_m/[1 + (\omega\tau_m)^2] + [P_2(\cos\theta_{ij,kl}) - S_{ij,kl}^2]\tau/[1 + (\omega\tau)^2]$$

$$j_{A,A}(\omega) = S^2\tau_m/[1 + (\omega\tau_m)^2] + [1 - S^2]\tau/[1 + (\omega\tau)^2]$$

Γ_{AX}, $\Gamma_{AX,A}$ and $\Gamma_{AX,AX}$ can be derived from substitution of M for X. In the above equations, τ_m is the overall rotational time; $1/\tau = 1/\tau_m + 1/\tau_e$ where τ_e is the effective correlation time of internal motion; $S_{ij,kl}^2$ is the cross-correlation order parameter; $P_2(\cos\theta_{ij,kl}) = 0.5(3\cos^2\theta_{ij,kl} - 1)$ where $\theta_{ij,kl}$ is the angle between vectors ij and kl; for auto-correlation (i.e., ij = kl), S_{ij}^2 are referred to as order parameter (S^2); σ_X, σ_Y and σ_Z are the principle components of the tensor along X, Y and Z axes; cosX, cosY and cosZ are the direction cosines of the AM or AX bond vector in the principle frame of ^{13}C CSA tensor. $j_{ij,i}$ is the spectral density for dipole-CSA cross-correlation and is assumed to be the same as $j_{A,A}$ and $j_{ij,ij}$ in our simulations, which is correct only when the internal motion is isotropic or the angle between the principal axis of the CSA tensor and the dipole is small (Ghose et al., 1998; Tjandra et al., 1996). R_{1Xsel} is the selective longitudinal relaxation rates of methylene protons. R_{ZQ} is the relaxation rate of zero-quantum coherence $X_{1+}X_{2-} + X_{1-}X_{2+}$. Both R_{1Xsel} and R_{ZQ} arise from dipolar interactions between methylene protons and their surrounding protons.

116

References

Bremi, T. and Bruschweiler, R. (1997) *J. Am. Chem. Soc.*, **119**, 6672–6673.

Brutscher, B., Bruschweiler, R. and Ernst, R.R. (1997) *Biochemistry*, **36**, 13043–13053.

Daragan, V.A. and Mayo, K.H. (1995) *J. Magn. Reson. Ser. B*, **107**, 274–278.

Daragan, V.A. and Mayo, K.H. (1997) *Prog. NMR Spectrosc.*, **31**, 63–105.

Daragan, V.A., Kloczewiak, M.A. and Mayo, K.H. (1993) *Biochemistry*, **32**, 10580–10590.

Delaglio, F., Grzesiek, S., Vuister, G.W., Zhu, G., Pfeifer, J. and Bax, A. (1995) *J. Biomol. NMR*, **6**, 277–293.

Eisenmesser, E.Z., Bosco, D.A., Akke, M. and Kern, D. (2002) *Science*, **295**, 1520–1523.

Emsley, L. and Bodenhausen, G. (1992) *J. Magn. Reson.*, **97**, 135.

Engelke, J. and Rüterjans, H. (1998) *J. Biomol. NMR*, **11**, 165–183.

Ernst, M. and Ernst, R.R. (1994) *J. Magn. Reson. Ser. A*, **110**, 202–213.

Fischer, M.W.F., Zeng, L., Pang, Y., Hu, W., Majumdar, A. and Zuiderweg, E.R.P. (1997) *J. Am. Chem. Soc.*, **119**, 12629–12642.

Frueh, D. (2002) *Prog. NMR Spectrosc.*, **41**, 305–324.

Garrett, D.S., Powers, R., Gronenborn, A.M. and Clore, G.M. (1991) *J. Magn. Reson.*, **95**, 214–220.

Ghose, R. and Prestegard, J.H. (1998) *J. Magn. Reson.*, **134**, 308–314.

Ghose, R., Huang, K. and Prestegard, J.H. (1998) *J. Magn. Reson.*, **135**, 487–499.

Kay, L.E. (1998) *Biochem. Cell Biol.*, **76**, 145–52.

Kay, L.E. and Bull, T.E. (1992) *J. Magn. Reson.*, **99**, 615–622.

Kay, L.E., Keifer, P. and Saarinen, T. (1992) *J. Am. Chem. Soc.*, **114**, 10663–10665.

Korzhnev, D.M., Billeter, M., Arseniev, A.S. and Orekhov, V.Y. (2001) *Prog. NMR Spectrosc.*, **38**, 197–266.

LeMaster, D.M. and Kushlan, D.M. (1996) *J. Am. Chem. Soc.*, **118**, 9255–9264.

Lipari, G. and Szabo, A. (1982) *J. Am. Chem. Soc.*, **104**, 4546–4559.

Liu, W.D., Zheng, Y., Cistola, D.P. and Yang, D.W., *J. Biomol. NMR*, in press.

London, R.E. and Avitabile, J. (1978) *J. Am. Chem. Soc.*, **100**, 7159–7165.

Mayne, C.L., Grant, D.M. and Alderman, D.W. (1976) *J. Chem. Phys.*, **65**, 1684–1695.

Millet, O., Muhandiram, D.R., Skrynnikov, N.R. and Kay, L.E. (2002) *J. Am. Chem. Soc.*, **124**, 6439–6448.

Montelione, G.T., Lyons, B.A., Emerson, S.D. and Tashiro, M. (1992) *J. Am. Chem. Soc.*, **114**, 10974–10975.

Muhandiram, D.R., Yamazaki, T., Sykes, B.D. and Kay, L.E. (1995) *J. Am. Chem. Soc.*, **117**, 11536–11544.

Nesmelova, I., Krushelnitsky, A., Idiyatullin, D., Blanco, F., Ramirez-Alvarado, M., Daragan, V.A., Serrano, L. and Mayo, K.H. (2001) *Biochemistry*, **40**, 2844–2853.

Palmer, A.G. (2001) *Annu. Rev. Biophys. Biomol. Struct.*, **30**, 129–155.

Palmer, A.G., Williams, J. and McDermott, A. (1996) *J. Phys. Chem.*, **100**, 13293–13310.

Pervushin, K., Riek, R., Wider, G. and Wüthrich, K. (1997) *Proc Natl. Acad. Sci. USA*, **94**, 12366–12371.

Prestegard, J.H. and Grant, D.M. (1978) *J. Am. Chem. Soc.*, **100**, 4664–4668.

Redfield, A.G. (1957) *IBM J. Res. Dev.*, **1**, 19.

Reif, B., Hennig, M. and Griesinger, C. (1997) *Science*, **276**, 1230–1233.

Tjandra, N., Szabo, A. and Bax, A. (1996) *J. Am. Chem. Soc.*, **118**, 6986–6991.

Wand, A.J. (2001) *Nat. Struct. Biol.*, **8**, 926–931.

Werbelow, L.G. and Grant, D.M. (1975) *J. Chem. Phys.*, **63**, 544–557.

Yang, D.W., Konrat, R. and Kay, L.E. (1997) *J. Am. Chem. Soc.*, **119**, 11938–11940.

Yang, D.W., Mittermaier, A., Mok, Y.K. and Kay, L.E. (1998a) *J. Mol. Biol.*, **276**, 939–954.

Yang, D.W., Tolman, J.R., Goto, N.K. and Kay, L.E. (1998b) *J. Biomol. NMR*, **12**, 325–332.

Ye, C., Fu, R., Hu, J., Hou, L. and Ding, S. (1993) *Magn. Reson. Chem.*, **31**, 699–704.

Zhang, F.L., Lucke, C., Baier, L.J., Sacchettini, J.C. and Hamilton, J.A. (1997) *J. Biomol. NMR*, **9**, 213–228.